THE ASTRONOMICAL JOURNAL, 120:2471–2487, 2000 November

THE LOW-RESOLUTION DRAO SURVEY OF H I EMISSION FROM THE GALACTIC PLANE

L. A. HIGGS AND K. F. TAPPING
National Research Council of Canada, Herzberg Institute of Astrophysics, Dominion Radio Astrophysical Observatory, Box 248, Penticton, B.C., Canada V2A 6K3; Lloyd.Higgs@nrc.ca
Received 2000 July 17; accepted 2000 July 31

ABSTRACT

A survey of H I line emission in the Galactic plane from Galactic longitude $l = 72.^{\circ}2$ to $149.^{\circ}0$, and latitude $b = -5.^{\circ}4$ to $7.^{\circ}2$, has been made using the 26-m Telescope at the Dominion Radio Astrophysical Observatory. Spectra were observed at $0.^{\circ}2$ intervals of longitude and latitude, providing a survey which is fully sampled in the spatial domain. A detailed study of the antenna characteristics of the telescope allowed the correction of the spectra for stray radiation. The spectral resolution is 1.32 km s^{-1}, and the LSR velocity range is -260 to 161 km s^{-1}. The final spectra have an estimated T_b scaling accuracy of 1% and an estimated rms noise in one channel (0.8245 km s^{-1}) of 0.25 K. A region of suspected strong H I self-absorption at $l \sim 92^{\circ}$, $b \sim 3^{\circ}$, has been identified. Comparison with spectra from the Leiden/Dwingeloo Survey is used to estimate the overall accuracy of the stray radiation corrections. This comparison also shows that a small percentage ($\sim$1%) of the spectra in the latter survey suffer from calibration errors exceeding 10%. A table of positions of the more discordant spectra is given.

Key words: Galaxy: kinematics and dynamics — ISM: H I — radio emission lines — surveys

1. INTRODUCTION

In 1995, a consortium of astronomers from Canadian and international institutions launched the Canadian Galactic Plane Survey (CGPS), a project to map a large portion of the northern Galactic plane in radio continuum and 21 cm hydrogen-line emission using the Synthesis Telescope at the Dominion Radio Astrophysical Observatory (DRAO), and at other wavelengths using data from other telescopes (Taylor et al. 2000). Observations made with the DRAO Synthesis Telescope lack information corresponding to interferometer spacings less than about 13 m. This has to be acquired with a large, single-aperture radio telescope. Ideally, these "short-spacing data" should be acquired using a radio telescope with an aperture of at least 40 m diameter, about 4 times the diameter of the individual antennas of the Synthesis Telescope. However, an H I survey made with such a telescope of the large area of sky to be covered by the CGPS did not exist, and the amount of observing time required to carry out such a survey would be difficult to obtain. Observations with a smaller telescope had to suffice. One possibility would be to use the recently completed Leiden/Dwingeloo Survey of Galactic H I (LDS) (Hartmann & Burton 1997), made with the 26-m Telescope at Dwingeloo. This survey has high sensitivity and good velocity coverage but is spatially undersampled. It was therefore decided to make a new, well-sampled survey using the 26-m Telescope at DRAO. This "Low-Resolution DRAO Survey of H I Emission from the Galactic Plane" (LRDS) was started in 1997.

The CGPS, in its original conception, was to image H I emission from the Galactic plane between longitudes $74.^{\circ}2$ and $147.^{\circ}3$, and between latitudes $-3.^{\circ}6$ and $5.^{\circ}6$. In order to extract accurately the short-spacing information, the area to be covered by observations with the DRAO 26-m Telescope had to be somewhat larger. It was decided that the LRDS should consist of spectral observations every $0.^{\circ}2$ of Galactic longitude and latitude between longitudes $72.^{\circ}2$ and $149.^{\circ}0$, and between latitudes $-5.^{\circ}4$ and $7.^{\circ}2$, i.e., 24,640 spectra. Although the LRDS was specifically carried out as a complementary survey to the CGPS, the resulting data will undoubtedly be of interest for other investigations of the Galaxy.

The survey project consisted of two parts: obtaining the observational data, and correcting the observed spectra for instrumental effects. Each of these will be discussed in turn.

2. OBSERVATIONS

2.1. *The 26 Meter Telescope and Receiver*

The 26-m Telescope at DRAO is a deep paraboloidal ($f/D = 0.3$) antenna, with a mesh surface, and with the receiver box supported at the focus on three feed-legs which are at an angle of $33.^{\circ}5$ to the antenna boresight. The effects of these feed-legs on observed spectra will be discussed later. The receiver used for the H I spectral-line observations uses an uncooled FET amplifier giving a system temperature of about 60 K at the zenith. Two orthogonal linear polarizations are observed independently. The telescope, on an equatorial mount, has an estimated rms pointing accuracy of $0.^{\circ}8$.

A three-level autocorrelation spectrometer produces 512 channel spectra of a 2 MHz bandwidth, in a frequency-switched observing mode (switching every 5.625 s). For the LRDS, each survey point was observed for 90 s, 45 s at the H I frequency and 45 s at a reference frequency 2 MHz lower. After averaging both polarizations, the resulting noise in a channel of width 0.824 km s^{-1} was about 0.17 K. A Gaussian taper which is applied to the correlation coefficients before inversion to the frequency domain yields a spectral resolution of 1.319 km s^{-1}. The spectra cover an LSR velocity range of -260 to 161 km s^{-1}.

2.2. *Observations and Calibration*

An observing scheme was devised that allowed frequent calibration of the receiver with a noise source and calibration against a standard IAU Galactic H I region, S7, which has a peak spectral-line brightness temperature of about 100 K (Williams 1973; Kalberla, Mebold, & Reich 1982). The grid of observing positions was covered in a

TABLE 1

BASIC PARAMETERS OF THE SURVEY

Parameter	Value
Spatial resolution (arcmin)	36
Spacing of spectra in l and b (arcmin)	12
Number of spectra	24,640
Channels per spectrum	512
Spectral resolution (km s^{-1})	1.319
Channel separation[a] (km s^{-1})	0.8245
LSR velocity range (km s^{-1})	−260 to 161
Integration time[b] (s)	90
rms noise (T_b^*) in one channel[c] (K)	0.17
rms noise (T_b) in one channel[d] (K)	0.25
rms distortion error[e] (%)	4.6
Accuracy of T_b scale (%)	~1

[a] Spectra are presented in velocity-channel format, but equally spaced frequency channels are output from spectrometer. Actual separation in km s^{-1} varies but velocity error so introduced is less than 0.07 km s^{-1} in end channels.

[b] Total frequency-switched time; time on H I line is 50% of this.

[c] This corresponds to 0.19 K in T_b considering only receiver noise.

[d] Estimated σ including effects of nonlinearity, pointing, and stray radiation corrections.

[e] Estimated error in channels on edges of features. The estimated uncertainty in peak line brightness is closer to 1%.

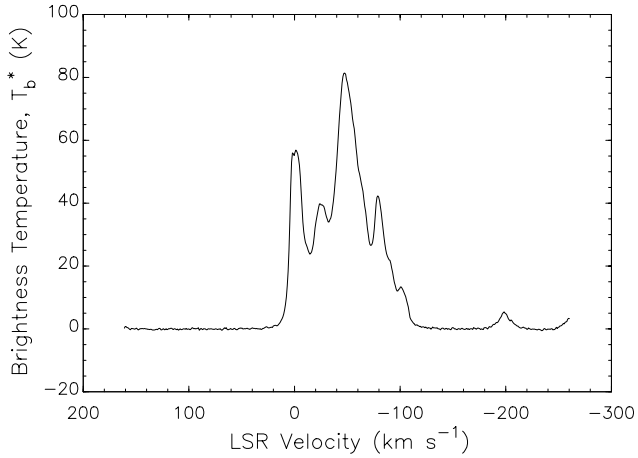

FIG. 1.—Observed H I spectrum at $l = 131.^{\circ}2$, $b = 1.^{\circ}0$. The rise in spectral intensity at the right-hand end of the spectrum ($V_{LSR} < -240$ km s^{-1}) is an artifact introduced by the correlator. A well-known "high-velocity cloud" can be seen at $V_{LSR} = -200$ km s^{-1} (Wakker & van Woerden 1991, Complex H).

series of "Galactic latitude scans" (typically two or three a day) where each "scan" (which is really a sequence of antenna pointings) consisted of the following:

A "noise observation" at the S7 position.

A spectral observation of S7.

A "noise observation" at the S7 position.

A "noise observation" at the first latitude position.

Thirty-two spectral observations at different latitudes, in 12′ steps. Scans can either be in increasing Galactic latitude or decreasing Galactic latitude.

A "noise observation" at the mid-latitude of the scan.

Thirty-two spectral observations a different latitudes, in 12′ steps.

A "noise observation" at the last latitude of the scan.

A "noise observation" at the S7 position.

A spectral observation of S7.

A "noise observation" at the S7 position.

Each scan produced 64 survey spectra at a given Galactic longitude, and 385 scans covered the LRDS area. A scheduling program ensured that each scan was observed with the telescope in the elevation range of 30°–60° (to minimize the effects of changing ground radiation) and that longitudes of the survey area were observed in a rather random fashion (to randomize any time-variable effects in the observing system).

The survey was started in 1997 April; by 1998 January, the collection of spectra was complete. A summary of the observational parameters of the LRDS is given in Table 1.

Calibrating the spectra was a two-stage process. First, spectral intensities were calibrated in terms of a noise signal injected into the receiver front end. This was assumed to have a constant antenna temperature, ~40 K, across the spectral band. These "noise observations" were made at the beginning, middle and end of each scan. Each noise observation, 180 s in duration, cycled through four states: observing (1) the H I band with the noise source turned on, (2) the H I band with the noise source turned off, (3) the reference band with the noise source turned on, and (4) the reference band with the noise source turned off. A database of calibration parameters was created from all the noise observations. This was then used to correct the observed spectra for band-shape effects and to calibrate the intensity scale in terms of the antenna temperature of the injected noise signal. Details are given in Appendix A.

The S7 spectral observations, and accompanying noise observations, were used to create a second database of calibration parameters which gave the effective brightness temperature (T_b^*) of the injected noise signal, on the assumption that the effective brightness temperature at the peak of the S7 spectrum was 100 K.

In the second calibration stage, factors from the S7 calibration database were used to convert the spectra to intensities expressed as T_b^*. Opacity corrections were made assuming a zenith opacity of 0.8% at the H I frequency. Spectra were then checked for interference, with affected channels being replaced by interpolated data. Any remaining base-level curvature was removed by fitting polynomials of order three or less to channels free of H I emission. The spectra in the two polarizations were then averaged.

A typical calibrated spectrum is shown in Figure 1, which presents the observation at $l = 131.^{\circ}2$, $b = 1.^{\circ}0$. The rise in the spectrum at the extreme right is an artifact introduced by the correlator.

2.3. *Repeatability*

During the course of the LRDS, several of the Galactic latitude scans were repeated. This gave an opportunity to check the repeatability of the observations. For example, the scan at $l = 140^{\circ}$ was observed in 1997 August (53 spectra) and again in 1997 October (64 spectra). The 53 spectra observed more than once were differenced, after they had been corrected for "stray radiation" contributions (see § 3), to give an estimate of the repeatability. It was found that the differences in spectral channels with $T_b > 10$ K had an estimated standard deviation, σ, of 0.44 K or 1.6%, whichever is less. Below $T_b = 10$ K, the σ was found to be 0.27 K. (This latter value is just what one would expect

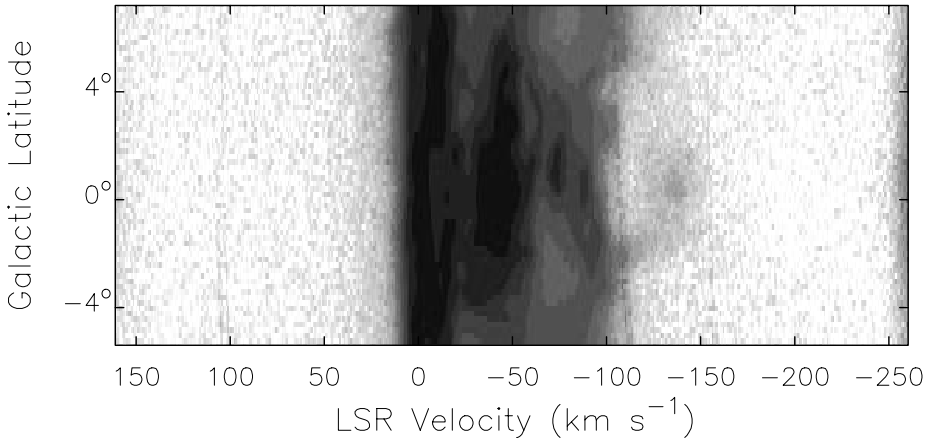

FIG. 2.—Observed H I spectra at $l = 140\overset{\circ}{.}0$, at the 64 Galactic latitudes comprising a latitude scan. The gray scale runs nonlinearly from 0 K (*white*) to 40 K (*black*), emphasizing low intensities. Faint artifacts resulting from incomplete removal of interference can be seen. Traces of the two locally produced signals can be seen at ~ 102 km s^{-1} and at ~ -158 km s^{-1}. The latter signal, before excision, peaked at about 5 K while the residual artifacts are below 0.25 K. A stronger interfering signal, reaching 6 K or more, at ~ -109 km s^{-1} has left stronger artifacts (~ 1.5 K) because the interference affected more than two channels.

in the difference of two spectra each having $\sigma = 0.19$ K, as indicated in the footnote to Table 1).

At this point in the calibration process, the scatter in the calibration parameters was estimated to produce an uncertainty in the temperature scale of the spectra of $\sim 1\%$. However, the spectra were affected by interference, possible nonlinearities in the receiver system, and the contamination of the observed spectra by extraneous spectral emission entering the feed from outside the main beam of the antenna ("stray radiation"). All of these effects required consideration.

2.4. *Interference*

The spectra were automatically checked for interference during the last stage of processing. Since most interference detected at DRAO in the H I band is quite weak, no more than two spectral channels are generally affected. The technique used to remove interference automatically, and to log it, is outlined in Appendix B. Most interference was found to occur near two laboratory frequencies: 1419.978 ± 0.014 and 1421.208 ± 0.005 MHz. These were eventually identified as arising in the correlation system in the DRAO Space VLBI laboratory, which is situated very close to the 26-m Telescope. Fortunately, these frequencies generally lie outside the spectral region of interest.

The automatic process for excising interference was found to be adequate for the main purpose for the LRDS—providing short-spacing data for the CGPS. Interference features appear as high spatial frequency features in channel maps and are subsequently filtered out in the short-spacing data extraction process. Some weak artifacts remain in a few spectra at the ~ 1 K level, especially in cases where the interfering signal appeared in more than two adjacent channels. These artifacts are easily recognized by examining all spectra for a given latitude scan. Figure 2 shows an intensity plot of 64 spectra at $l = 140°$ in which such artifacts are visible. This is probably the worst case of interference artifacts which remain in the survey data. (The fourth panel of Fig. 15 shows evidence of weak interference near -168 km

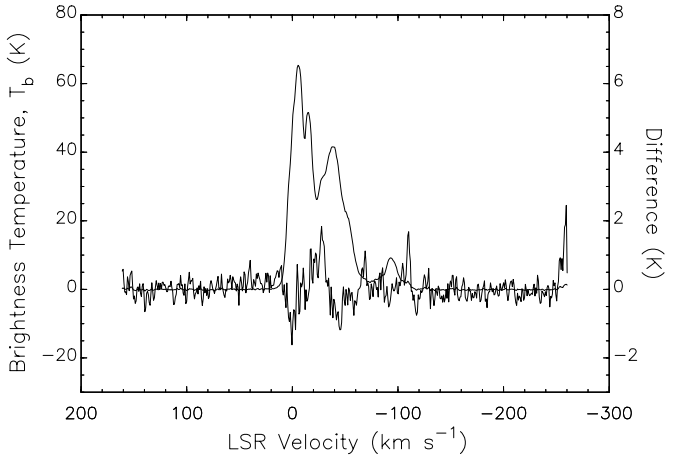

FIG. 3.—Corrected (for stray radiation) H I spectrum at $l = 140\overset{\circ}{.}0$, $b = -3\overset{\circ}{.}0$, which was observed in 1997 October. The heavy line (using the right-hand scale) gives the difference between this spectrum and the corrected version of one observed in 1998 May after the receiver was made more linear. The "spike" in the difference at -110 km s^{-1} corresponds to the interference shown in Fig. 2, which was present only in the 1997 spectrum.

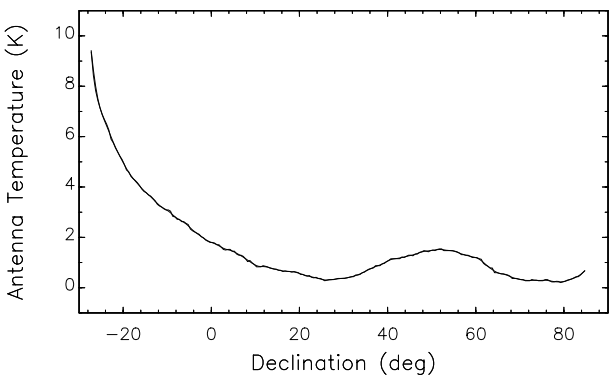

FIG. 4.—Lower envelope of 30 scans along the meridian. This was subtracted from observed scans to derive the contributions to antenna temperature resulting from the Sun in antenna sidelobes. The rise in antenna temperature near the zenith (decl. = 49°) results from the spillover lobe being directed toward the ground.

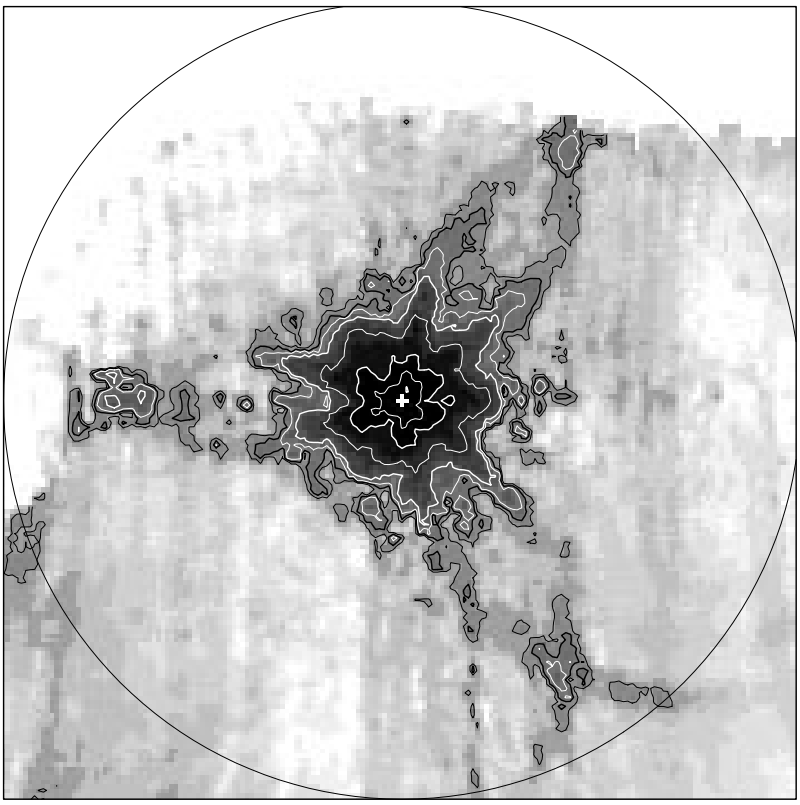

FIG. 5.—Observed antenna pattern within 45° of the main beam (*white cross at center of figure*). The outer circle indicates $\theta_d = 45°$. The contour levels are −49 dB (*black*), −48 dB (*heavy black*), −47 dB (*white*), −45 dB (*heavy white*), −40 dB (*white*), −35 dB (*heavy white*), −30 dB (*white*), and −25 dB (*heavy white*). The unobserved region across the top of the figure results from the Sun's low declination (i.e., it is the southern horizon cutoff), while the unobserved top left-hand corner corresponds to the presence of emission from the Galactic plane in the main beam. The average level at the crossover points of the scatter cones, at $\theta_d \sim 34°$, is found to be about −45.2 dB. The vertical striping is a consequence of difficulties in background removal.

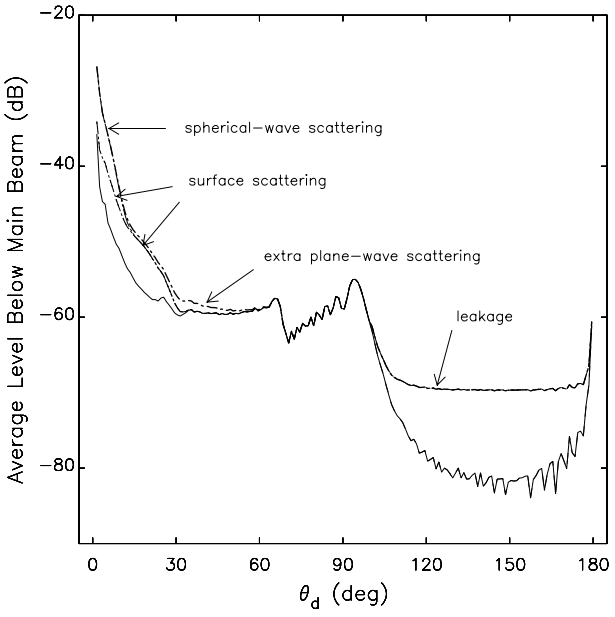

FIG. 6.—Azimuthally averaged pattern levels as a function of θ_d. The light lower curve gives the result of the electromagnetic computations, while the upper curves (*various dot-dash combinations*) show the contributions of extra scattering or loss mechanisms, as indicated. The upper envelope corresponds to the pattern shown in Fig. 7.

s^{-1} that persisted for many latitude scans at different longitudes.)

2.5. *Nonlinearity of Receiver/Spectrometer*

The wide range of signal levels encountered in the survey, and the nature of the digital processing involved in generating the spectra, make linearity of the receiver/spectrometer system very important. Accordingly, before starting the LRDS in 1997, measurements were made of the linearity. Strong continuum sources were used. It was found that the system was slightly nonlinear in that the response to the noise calibration was reduced by about 15% when the antenna was directed at Cas A, which increased the antenna temperature by ∼180 K. For the differences in antenna temperature predicted during the LRDS, the expected nonlinearity would not exceed a few percent, which was deemed acceptable. It should be noted that the effects of any nonlinearity are removed to a first order by the frequent direct calibration against S7. The nonlinearity inherent in the three-level spectral correlator is corrected in software (Hovey 1998).

After the LRDS was completed in the spring of 1998, a second series of calibration observations on strong radio-continuum sources showed that the receiver/spectrometer nonlinearity had increased. After considerable investigation, this was found to be due to incorrect power levels

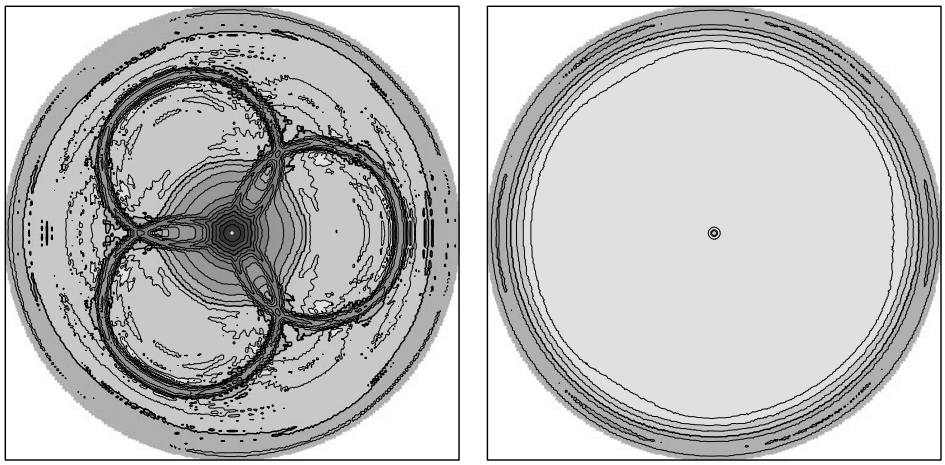

FIG. 7.—Adopted antenna pattern for the DRAO 26-m Telescope. *Left*: Front hemisphere; *right*: rear hemisphere. In the left-hand section of the figure, the scatter cones resulting from the scattering by the feed-legs of the plane wave emanating from the aperture are clearly seen, while the spillover lobe can be seen in the right-hand section. The contour levels run from −32.5 to −67.5 dB, in steps of 2.5 dB. The main beam is the white dot in the center of the left-hand section.

feeding the single-sideband (baseband) mixers, which necessarily include a combination of very lossy and high-gain components. The levels were corrected, and two LRDS scans (at $l = 140\overset{\circ}{.}0$ and $l = 140\overset{\circ}{.}8$) were repeated to evaluate errors in line shape that might have resulted from the nonlinearity.

Some changes were found in the observed spectra. However, these were comparable to the variation in stray radiation corrections (see § 3) with the date of observation, so the spectra were corrected for stray radiation before detailed comparisons were made. Based on the 128 repeated spectra, it was found that the differences in brightness temperature, T_b, in channels with $T_b > 10$ K had an estimated standard deviation of 0.88 K or 2.9%, whichever is less, while the estimated σ for the differences in the weaker channels was 0.32 K. These exceed the corresponding numbers for repeatability noted in § 2.3, indicating that nonlinearity did cause some errors in line shape.

It would be very difficult to remove the effects of nonlinearity from the observed spectra, so it was decided that these uncertainties could be accepted. In Figure 3, an example of the resulting differences is presented. This shows the LRDS spectrum at $l = 140\overset{\circ}{.}0$, $b = -3\overset{\circ}{.}0$ (corrected for stray radiation) and the difference between it and a corrected spectrum observed after the receiver was made more linear.

3. STRAY RADIATION CORRECTIONS

By far the biggest correction required in order to produce accurate spectra is the so-called stray radiation correction (Kalberla 1978; Kalberla, Mebold, & Reich 1980). Since H I line emission comes from all parts of the observable sky, a significant amount is received through the antenna sidelobes. The observed spectrum is therefore not an accurate representation of the H I emission received in the main beam of the telescope. To correct for this effect, one must know the spatial and frequency distribution of H I emission over the visible sky at the time of observation and have a good knowledge of the properties of the telescope (aperture and beam efficiencies, and the full sidelobe structure of its antenna pattern). Before the LRDS, the properties of the DRAO 26-m Telescope were only approximately understood, so an important part of the LRDS project was to improve the knowledge of the antenna parameters.

3.1. *Measurement of Antenna Parameters*

Some rudimentary measurements of the forward antenna pattern of the 26-m Telescope were made shortly after its construction (Hanson 1964), but the full antenna pattern has never been measured. Lacking a suitable site in the far field (>6 km away) for a transmitter to be used to measure directly at least half of the pattern, it was decided to define the pattern through a combination of computation and measurement. Using known geometrical parameters for the antenna, feed-legs, and focus box, and the measured pattern of the antenna feed, an electromagnetic software package (NEC 1982) was used to compute the first approximation of the telescope response. This code modeled the aperture blockage due to the feed-legs (scattering of the plane wave emerging from the reflector, in the transmitting case, into "scatter cones") and due to the focus box. It did not, however, allow for leakage through the mesh surface of the antenna, scattering by irregularities in the antenna surface, and the scattering, by the feed-legs, of the spherical wave emerging from the antenna feed. For a deep antenna with feed-legs based well inside the aperture, such as the DRAO telescope, the latter factor is very important. Moreover, the theoretical calculations for the plane-wave scattering assumed cylindrical feed-legs rather than their actual "cigar-like" geometry.

These three missing loss mechanisms were investigated and estimates were made of their contribution to antenna efficiency and of the redistribution of the scattered radi-

ation. To discuss this, it is clearest to treat the antenna as if it were transmitting radiation, which is symmetrically equivalent to the receiving case. Definitions of the antenna parameters referenced in this paper are given in Appendix C.

The leakage efficiency, η_l, represents a small loss and could adequately be estimated from the mesh dimensions and standard reference sources. The redistribution of the lost power is not of great consequence since in astronomical observations it usually falls on the ground, not the sky!

The surface-scattering efficiency, η_{ss}, is related to a characteristic amplitude, δ, of the surface irregularities by the Ruze equation

$$\eta_{ss} = e^{-(4\pi\delta/\lambda)^2} , \quad (1)$$

where λ is the wavelength. From past measurements of the aperture efficiency of the 26-m Telescope at several frequencies, it is possible to deduce that $\delta = 0.45 \pm 0.03$ cm, and hence that $\eta_{ss} \approx 0.93$. The power scattered from the reflector surface is redistributed into some sort of Gaussian "plateau" underlying the main beam in a way which depends upon the (unknown) details of the surface irregularities.

A ray-tracing analysis of the spherical-wave scattering has shown that about 7% of the power emitted by the feed is scattered by the feed-legs before reaching the main reflector. Combining this with the corresponding loss in aperture illumination leads to a prediction that the spherical-wave–scattering efficiency, η_{sw}, is about 0.86. This energy is scattered into a roughly triangular region (because of the three feed-legs) near the main beam.

In order to define better these last two efficiency factors (which account for nearly 20% of the losses from the main beam) and the redistribution of the scattered radiation, measurements of the region surrounding the main beam were made using the Sun as a "point" source of emission. The procedure adopted was similar to that used (Murphy 1993) to measure the pattern of the NRAO 140 foot (43 m) telescope.

Rapid scans were made from the horizon to the pole and back, along the north-south meridian, as the Sun moved across the sky. The lower envelope of the recorded power levels, resulting from varying ground and atmospheric emission, was subtracted from the observed antenna temperatures, leaving only contributions from the Sun in the antenna sidelobes and celestial sources in the main beam. The latter were edited from the data, and the former were converted to measurements of sidelobe levels (using calibration observations with the Sun in the main beam, with suitable calibrated attenuation). A derived "background" scan (the lower envelope of 30 scans) is shown in Figure 4, and the resulting observed antenna pattern is shown in Figure 5. This technique was only useful for measuring sidelobe levels stronger than -50 dB (with respect to the main beam), being limited by receiver noise and instabilities in the technique itself. The spillover lobe, estimated to be weaker than -55 dB, was not observable, and the "scatter cones" were only measurable near the main beam.

The magnitude and distribution of the efficiency terms missing from the theoretical calculations were determined with the aid of a comparison of the observed antenna pattern in Figure 5 with the computed pattern. After much trial-and-error experimentation, a set of antenna parameters was found that was consistent with the observations of Figure 5 (but only marginally consistent with Fig. 4). The modifications added to the theoretical pattern are presented schematically in Figure 6, which shows azimuthally averaged (over ϕ_d) pattern levels, before and after the addition of the extra terms. The antenna pattern finally adopted for stray radiation computations is shown in Figure 7. The

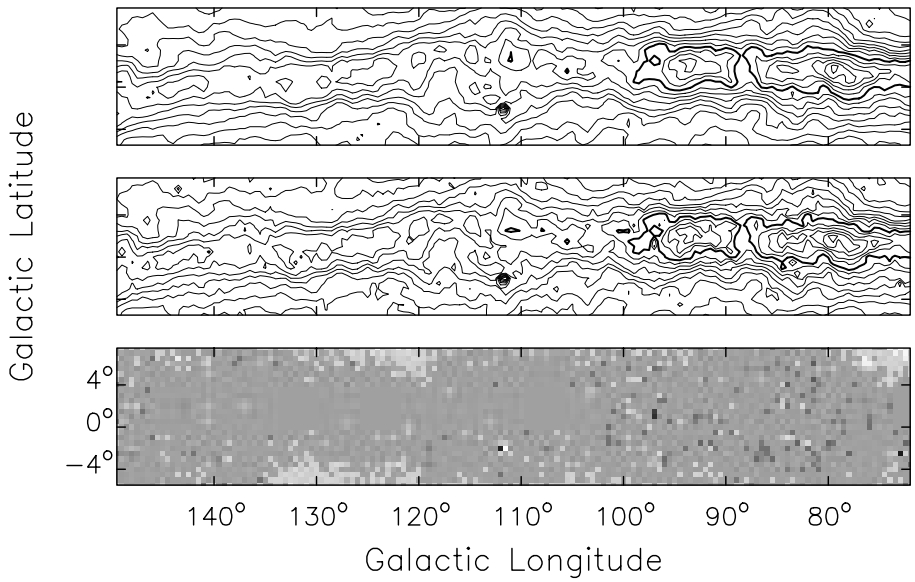

FIG. 8.—*Top*: Integrated H I line, -200 km s$^{-1} \leq V_{LSR} \leq 100$ km s^{-1}, from the LRDS, after interpolation onto the LDS observing grid. The contours are in steps of 500 K km s^{-1}, from 500 to 7500 with every second contour heavier. The heaviest contour is at 5000 K km s^{-1}. The deep depression at $l = 112°$, $b = -2°$, is due to absorption of continuum emission from Cas A, while the weaker depression at $l = 76°$, $b = 6°$, results from Cyg A. *Middle*: A similar plot for the LDS spectra. The overall distribution is the same but the contours indicate additional "noise." *Bottom*: The ratio of the above two plots (LRDS/LDS) presented as a gray scale. The dominating gray level indicates a ratio, R, in the range $0.95 \leq R \leq 1.05$. Darker pixels have $R > 1.05$ in steps of 0.1, while lighter areas have $R < 0.95$, again in steps of 0.1. The Galactic coordinates for all three panels are as shown for the bottom panel.

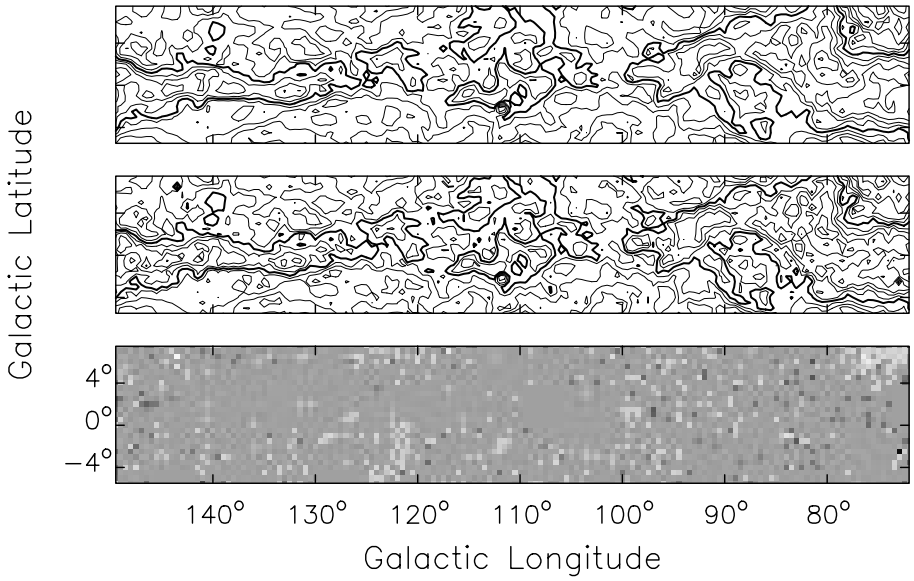

FIG. 9.—*Top*: Peak H I line intensity from the LRDS, after interpolation onto the LDS grid. The contours are in steps of 10 K, from 30 to 130 K with every second contour heavier. The heaviest contour is at 80 K. *Middle*: A similar plot for the LDS spectra. The overall distribution is the same but the contours indicate additional "noise." *Bottom*: The ratio of the above two plots (LRDS/LDS) presented as a gray scale. The dominating gray level indicates a ratio, R, in the range $0.95 \leq R \leq 1.05$. Darker pixels have $R > 1.05$ in steps of 0.1, while lighter areas have $R < 0.95$, again in steps of 0.1. The Galactic coordinates for all three panels are as shown for the bottom panel.

antenna parameters corresponding to this pattern are listed in Table 2. For the stray radiation calculations, average values of the antenna pattern were determined for 38,340 (θ_d,ϕ_d) cells, each about $1^\circ \times 1^\circ$, omitting the main beam.

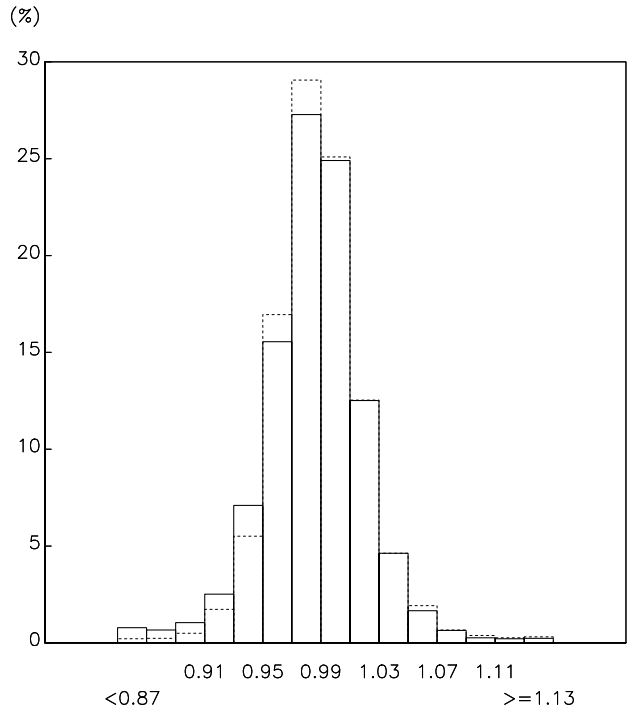

FIG. 10.—Histograms of the ratio distributions in the lower panels of Figs. 8 and 9. The solid bars give the histogram of integrated-intensity ratios, while the dotted bars give that for the peak-intensity ratios. The histograms show the percentage of pixels in the ratio plots that have given R values. The histogram boxes have a width of 0.02, and the boundary values of several are indicated. The two end boxes contain the outliers, $R < 0.87$ and $R > 1.13$.

3.2. *Creation of "True" H I Sky*

The existence of the Leiden/Dwingeloo Survey of Galactic H I (LDS) (Hartmann & Burton 1997) greatly simplified the problem of creating a database of H I spectra that represents the "true" H I sky. The LDS was corrected for stray radiation and covers nearly the whole sky visible from Penticton. For the computation of stray radiation corrections, it has been somewhat condensed into a special database. The sky was divided into 38,760 (l,b) cells, each about $1^\circ \times 1^\circ$, in a similar fashion to the gridded antenna pattern. The gridding of the LDS spectra into these cells was done by simply averaging (unweighted) the original LDS spectra whose pixel centers fell into these new spatial cells. The averaged spectra were then regridded into 256 channels of width 1.32 km s^{-1} centered at 0 km s^{-1}, using a simple weighted average of the original LDS channels falling within the new velocity cells.

Although it had been recognized that some of the LDS spectra had calibration errors (see § 4), no attempt was made to correct the spectra since such errors would have little effect on the computed corrections.

3.3. *Computation of Corrections*

The computation of stray radiation corrections was straightforward once the two databases had been prepared: the antenna pattern and true H I sky. A convolution of the latter by the former, with appropriate velocity shifting of the true sky spectra at each pixel, gave the antenna temperature contribution to the observed H I spectrum that came from outside the main beam. However, some care was required to convert this to the appropriate correction to convert the observed T_b^* spectra to true T_b spectra. The problem arises because the observational spectra were calibrated against an observed S7 spectrum, which itself is varying slightly because of differing stray radiation contributions.

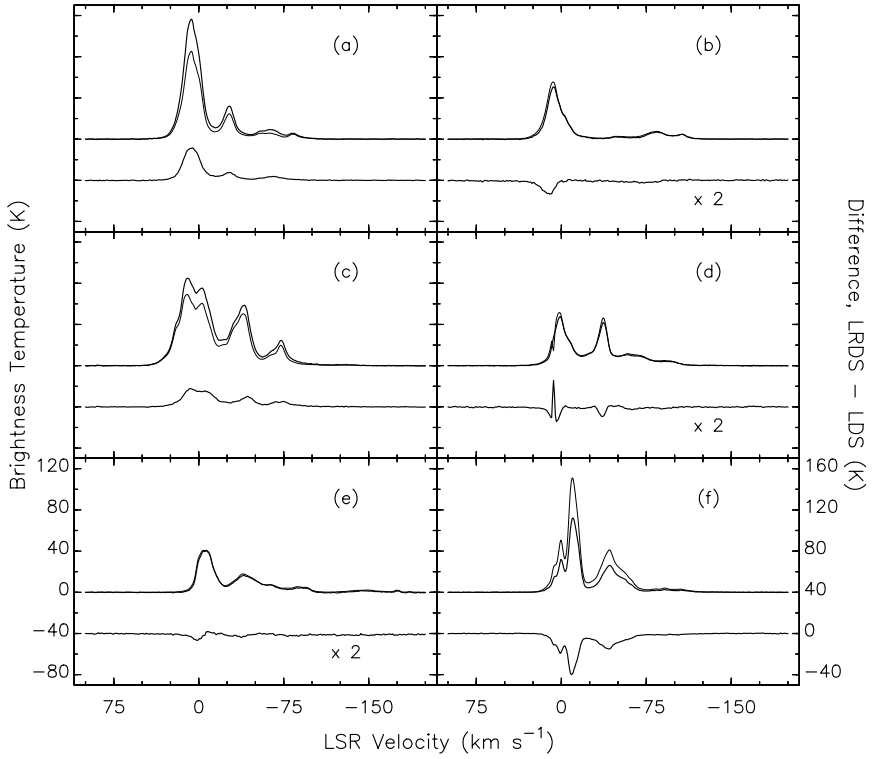

FIG. 11.—Comparison of LRDS and LDS spectra at selected positions where discrepancies have been detected. In each case, the LRDS spectrum is drawn heavier than the LDS spectrum, and the difference spectrum (LRDS − LDS, also heavy) is plotted below, to the same scale or magnified by 2. (*a*) $l = 73\overset{\circ}{.}0$, $b = -2\overset{\circ}{.}5$: an example where the LDS spectrum has been scaled too low. (*b*) $l = 74\overset{\circ}{.}0$, $b = 7\overset{\circ}{.}0$: an example where the stray radiation corrections seem to differ. (*c*) $l = 83\overset{\circ}{.}0$, $b = -1\overset{\circ}{.}5$: another example where the LDS spectrum has been scaled too low. (*d*) $l = 96\overset{\circ}{.}5$, $b = -4\overset{\circ}{.}0$: an example where there is a spurious "absorption" dip in the LDS spectrum. (*e*) $l = 132\overset{\circ}{.}0$, $b = -5\overset{\circ}{.}0$: another example where the stray radiation corrections seem to differ. (*f*) $l = 143\overset{\circ}{.}5$, $b = 6\overset{\circ}{.}5$: an example where the LDS spectrum has been scaled too high.

Fortunately, this is a small effect. The estimated peak antenna temperature observed on S7 with the DRAO telescope is 82.4 K, of which 8.29 K is a stray component which has a maximum variation (maximum − minimum) of 0.4 K. Ignoring the variation would introduce scaling errors of about 0.2%, much less than other calibration uncertainties. Therefore the variation in the observed S7 spectra due to stray radiation was ignored. If $ST(i)$ is the computed

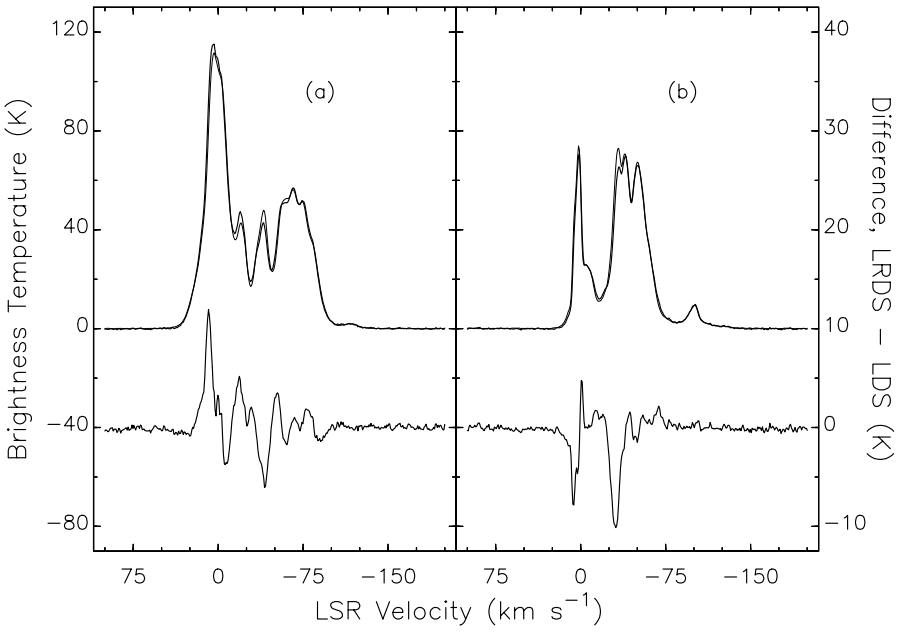

FIG. 12.—Two of the worst cases of differences between LRDS and LDS spectra which otherwise match well in terms of peak line brightness. In each case, the LRDS spectrum is drawn heavier than the LDS spectrum, and the difference spectrum (LRDS − LDS, also heavy) is plotted below, at four times the scale. (*a*) $l = 74\overset{\circ}{.}0$, $b = 1\overset{\circ}{.}0$: note the different ratio of the peaks at −19.5 and −40.1 km s^{-1} in the two surveys. (*b*) $l = 119\overset{\circ}{.}0$, $b = -1\overset{\circ}{.}0$: note the different ratio of the peaks at −33.5 and −39.7 km s^{-1} in the two surveys.

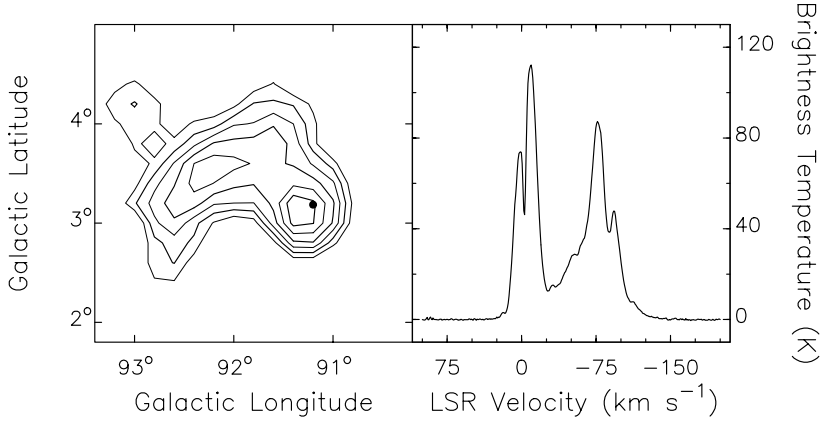

FIG. 13.—*Left*: A contour plot of $\sigma_{\rm est}$ in the only LRDS region where values exceeding 0.38 K are found. The contour levels run from 0.34 to 0.44 K in steps of 0.2 K. The black dot shows the location of the spectrum at the right. *Right*: The LRDS spectrum observed at $l = 91\overset{\circ}{.}2$, $b = 3\overset{\circ}{.}2$. Note the "absorption" dip at -4 km s^{-1}.

(predicted) antenna temperature in channel i due to stray radiation, the above antenna temperature predictions for S7, the beam efficiency in Table 2, and the requirement that the peak T_b on S7 be 100 K yield the following relationship between T_b^* and T_b:

$$T_b(i) = 1.1118T_b^*(i) - 1.3587ST(i)\ . \qquad (2)$$

Using equation (2), all observed spectra were then converted to calibrated T_b spectra. On an Intel P2 450-MHz processor operating under LINUX, the computation of each correction spectrum took 3.2 s.

4. COMPARISON WITH LEIDEN/DWINGELOO SURVEY

Since the Leiden/Dwingeloo Survey was also carefully corrected for stray radiation, a direct comparison of LDS spectra with LRDS spectra could provide a check on the accuracy of these corrections. The subset of the LDS in the area $l = 72\overset{\circ}{.}0$ to $149\overset{\circ}{.}5$, $b = -5\overset{\circ}{.}5$ to $7\overset{\circ}{.}5$, was selected for direct comparison with the LRDS results. Each of the 4212 LDS spectra in this region was regridded in velocity into the DRAO velocity channels. Unfortunately the sampling grid used for the LRDS only matched that of the LDS at whole degree values of l and b. At these points, the corrected LRDS spectrum was adopted as the DRAO "comparison" spectrum. For other LDS sample points, the DRAO "comparison" spectrum was obtained by quadratic interpolation using the nearest LRDS spectra (linear extrapolation at the edges of the above area). Each DRAO comparison spectrum was then compared with its LDS counterpart.

It was immediately discovered that there were severe discrepancies at a few positions in the Galactic plane, with peak H I brightness temperatures differing by 10%–40%. The question therefore arose as to which survey was to be considered more reliable in the case of discrepant spectra. In Figure 8, plots of the integrated H I line intensity (K km s^{-1}) over the range $-200 \le V_{\rm LSR} \le 100$ km s^{-1} are presented for the LRDS and the LDS, plus a plot of the ratio, LRDS/LDS. It can be seen that the distribution of integrated line intensity for the LRDS is considerably smoother than that for the LDS. The ratio plot shows that the two surveys generally agree well within $\pm 5\%$, but that there are numerous pixels where there are large differences. (The large ratio differences near Cas A are not unexpected since the detailed absorption spectrum on this strong source depends upon the aperture efficiency of the telescope and is affected by pointing errors.) Aside from these "random" discrepancies, there are indications of systematic differences, especially between $l = 120^\circ$ and 135° at latitudes below

TABLE 2

DERIVED ANTENNA PARAMETERS

Parameter	Symbol	Estimated Value
Radiative efficiency	η_r	0.995 ± 0.005[a]
Illumination efficiency	$\eta_{\rm ill}$	0.722 ± 0.009
Spillover efficiency	$\eta_{\rm spo}$	0.950 ± 0.005
Spherical-wave–scattering efficiency	$\eta_{\rm sw}$	0.874 ± 0.004
Leakage efficiency	η_l	0.9961 ± 0.0008
Surface-scattering efficiency	$\eta_{\rm ss}$	0.937 ± 0.009
Blockage efficiency	η_b	0.957 ± 0.003
Aperture efficiency	η_A	0.531 ± 0.009
Directivity	D_A	$(7.76 \pm 0.13) \times 10^4$
Antenna gain	G_A	$(7.72 \pm 0.14) \times 10^4$
Antenna solid angle (sr)	Ω_A	$(1.62 \pm 0.03) \times 10^{-4}$
Main-beam solid angle (sr)	$\Omega_{\rm MB}$	$(1.20 \pm 0.03) \times 10^{-4}$
Beam efficiency	η_B	0.736 ± 0.020
Stray factor	β	0.260 ± 0.020

[a] Undetermined. May be closer to 1.0.

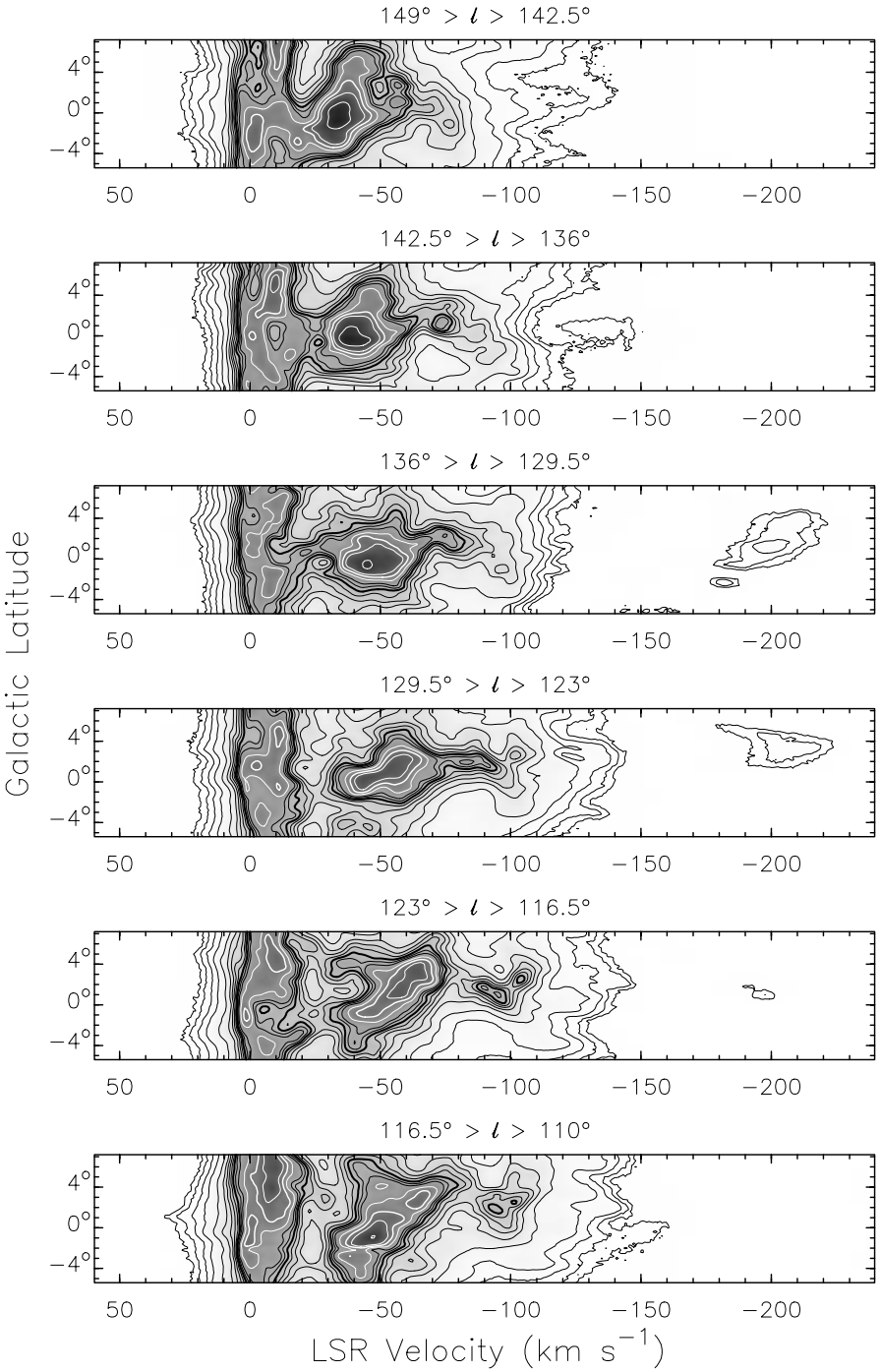

FIG. 14.—Average H I line brightness in six Galactic longitude intervals, as a function of LSR velocity and Galactic latitude. The contours are at levels of 0.25, 0.5, 1, 2, 5, 10, 15, 20, 25, 30, 35, 40, 50, 60, 70, 90, and 110 K, with every second contour plotted heavier. The heaviest black contour is at 30 K, and the heaviest white contour is at 60 K.

$-3°$, between $l = 120°$ and $130°$ at latitudes above $5°$, and in the region to the Galactic northwest of Cyg A. In these areas, the LRDS has systematically lower integrated intensities. This may indicate differences in the stray radiation corrections for the two surveys—the LDS may have been undercorrected or the LRDS may have been overcorrected.

A similar diagram for the peak line intensities is presented in Figure 9. Again, the LRDS plot is smoother than that for the LDS spectra. The ratio plot indicates that the two surveys are generally quite consistent but there are scattered pixels in which large differences appear. There seems to be less evidence for systematic differences, but the LRDS peak line intensities are definitely lower in the region to the northwest of Cyg A, $l \sim 73°$ and $b \sim 7°$.

The distribution of ratios in the lower panel of Figure 8 has a mean of 0.985 with a σ of 0.049. This indicates that the brightness temperature scales for the two surveys are concordant within $\sim 1\%$, but the scatter is a bit more than one would expect for the ratio of two surveys claiming internal accuracies of about 1%. Similar numbers for the distribution of ratios in the lower panel of Figure 9 are a mean of 0.989 and a σ of 0.034, indicating that the peak line inten-

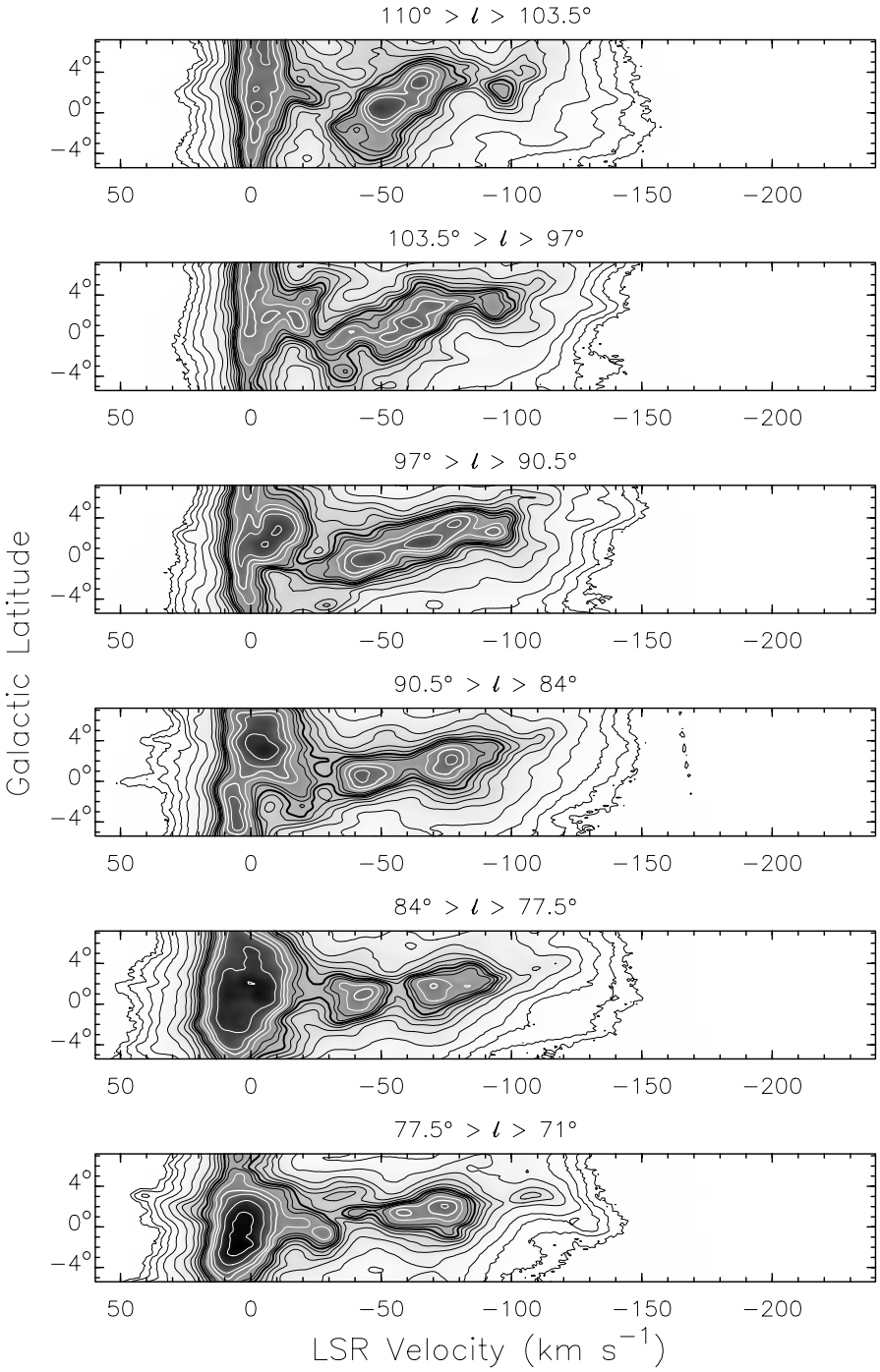

FIG. 15.—Average H I line brightness in six Galactic longitude intervals, as a function of LSR velocity and Galactic latitude. Contours are as in Fig. 14.

sities are slightly more consistent than the integrated line intensities. This may again reflect differences in the stray radiation corrections. A histogram of these distributions is presented in Figure 10.

The spectra at positions where major discrepancies appear between the LRDS and the LDS have been compared with spectra from the Weaver & Williams (1973) survey. Although the latter were not corrected for stray radiation, the comparison showed that in all such cases, the LRDS spectra agreed better than the LDS spectra. This is a strong indication that there are random scale errors in a small fraction of the LDS spectra. D. Hartmann (1999, private communication) has noted that broadband interference could have occasionally gone undetected during the LDS, causing calibration errors that could account for these discrepant spectra. From the statistics of Figure 9, perhaps 1.1% of the LDS spectra have scale errors of 10% or more (although a small fraction of these may result from differences in stray radiation corrections rather than scaling errors). In addition to these differences which appear to be mainly a scale difference, two LDS spectra were noted to have sharp apparent "absorption" dips which do not appear in their LRDS equivalents. These may also be the result of interference.

In Table 3, LDS spectra which have suspected scale errors of 10% or more, or discordant spectral features, are

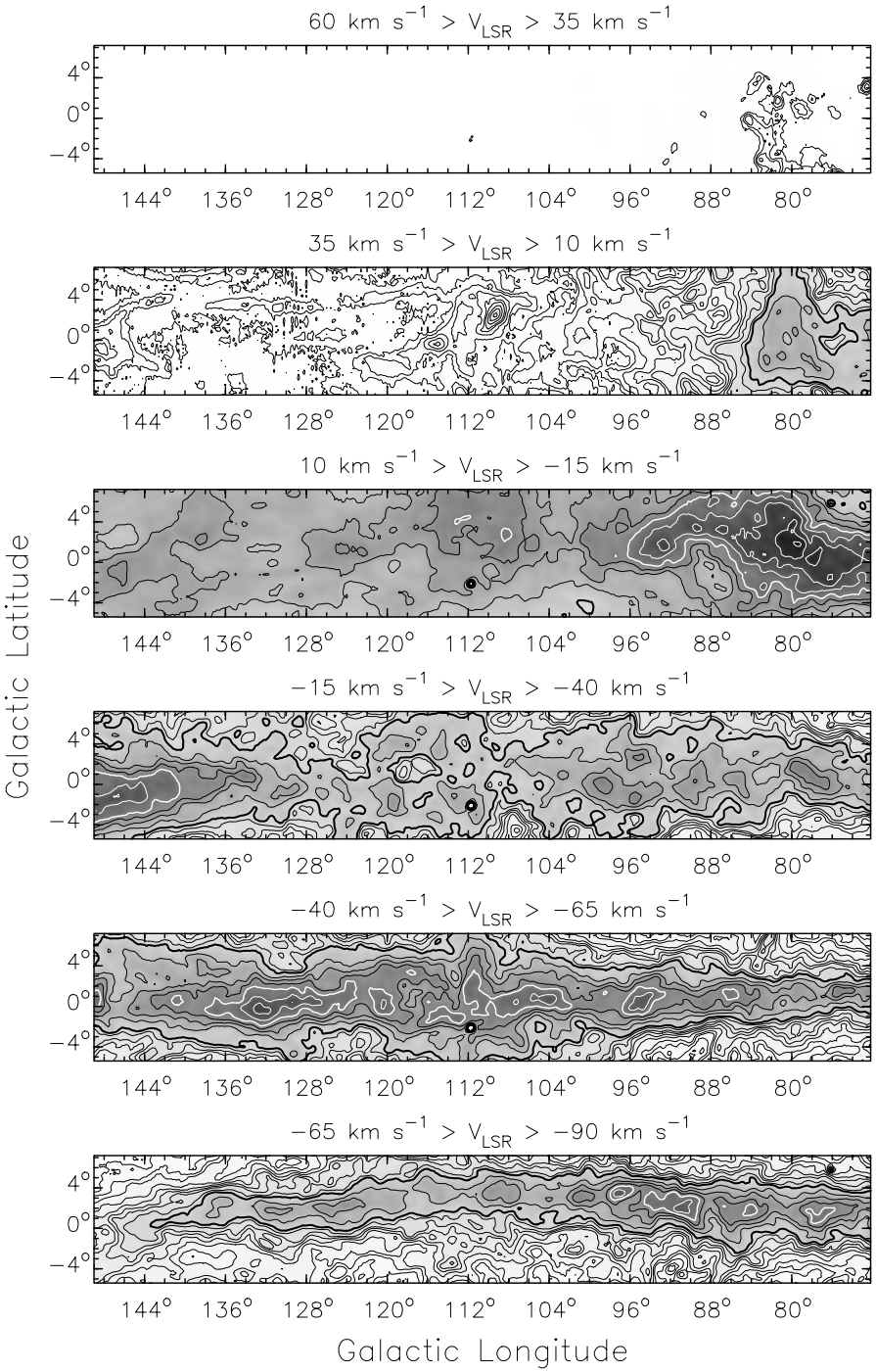

FIG. 16.—Integrated H I line intensity (K km s^{-1}) in six LSR velocity intervals, as a function of Galactic longitude and latitude. The contours are at levels of 10, 20, 30, 50, 75, 100, 150, 200, 250, 300, 400, 500, 750, 1000, 1250, 1500, 1800, 2100, 2400, and 2700 K km s^{-1}, with every second contour plotted heavier. The heaviest black contour is at 500 K km s^{-1}, and the heaviest white contour is at 1500 K km s^{-1}.

listed. These have been selected from the ratio plots in Figures 8 and 9, ignoring border pixels and regions where differences in stray radiation corrections may be affecting the ratios. Four sample spectra from this list, plus two cases where the stray radiation corrections may have differed for the two surveys (integrated line intensities differ by 12%), are shown in Figure 11.

5. DISCUSSION OF SURVEY RELIABILITY

It is useful to establish some criteria for the reliability of the LRDS spectra, allowing for the effects of the receiver nonlinearity, the uncertainty in the stray radiation corrections, and possible pointing errors.

The meager statistics of § 2.3 indicate that the observed spectra had an uncertainty (in T_b) of about 0.19 K in one channel and a "distortion" uncertainty of about 1.1% (after allowing for the conversion from *difference* statistics). These are estimates of σ and the distortion uncertainty is the maximum fractional error in line intensities to be expected in channels where the intensity exceeds 10 K. This maximum generally occurs on the edges of spectral features;

TABLE 3

LEIDEN/DWINGELOO SURVEY SPECTRA WITH SUSPECTED ERRORS

LONGITUDE (deg)	LATITUDE (deg)	RATIO (LRDS/LDS) Integrated Intensity	RATIO (LRDS/LDS) Peak Intensity	COMMENTS
72.5	−2.5	0.89	0.91	
73.0	−2.5	1.39	1.36	See Fig. 11*a*
73.5	6.0	0.90	0.90	
76.0	0.0	1.11	1.09	
79.0	1.5	1.09	1.11	
81.5	4.5	1.17	1.16	
81.5	6.0	1.17	1.17	
82.0	−2.0	1.11	1.10	
83.0	−1.5	1.24	1.23	See Fig. 11*c*
83.5	−0.5	1.12	1.09	
84.0	−2.0	1.10	1.08	
84.0	4.0	1.19	1.16	
84.5	−1.0	0.89	0.87	
85.5	−5.0	0.90	0.89	
89.5	−0.5	1.15	1.11	
90.5	−0.5	0.92	0.90	
91.0	−2.0	1.10	1.09	
91.0	1.0	0.91	0.90	
96.5	−4.0	...	...	Spurious feature; see Fig. 11*d*
96.5	5.5	1.13	1.10	
97.0	1.0	1.31	1.24	
97.0	1.5	1.26	1.22	
97.5	−4.0	...	...	Spurious feature
98.0	4.5	1.11	1.10	
99.0	1.5	0.92	0.89	
99.0	3.0	1.12	1.08	
99.5	−1.0	0.94	0.90	
99.5	2.5	0.91	0.90	
106.5.....	−3.0	0.85	0.87	
108.0.....	−3.5	0.85	0.87	
109.0.....	7.0	0.87	0.88	
112.0.....	−4.5	1.11	1.12	
112.5.....	6.5	0.89	0.90	
113.5.....	−4.0	0.89	0.89	
117.0.....	7.0	0.81	0.83	
122.5.....	−1.0	0.93	0.90	
124.5.....	7.0	0.88	0.95	
126.5.....	6.0	1.13	1.12	
131.5.....	6.5	0.90	0.93	
133.5.....	−4.0	0.88	0.92	
134.0.....	6.0	1.10	1.10	
134.5.....	−1.0	1.10	1.11	
134.5.....	6.5	0.85	0.86	
135.0.....	−4.5	0.90	0.89	
137.5.....	6.5	1.13	1.14	
140.5.....	0.5	0.88	0.88	
141.0.....	−4.5	0.86	0.89	
143.5.....	6.5	0.62	0.65	See Fig. 11*f*

the uncertainty in peak brightness temperatures is less than this. Allowance for nonlinearity (see § 2.5) raises these to 0.23 K and 2.1%, respectively.

To assess the reliability of the stray radiation corrections, the only course of action is to compare the spectra directly with those of another survey independently corrected for stray radiation, e.g., the LDS. From the data in the bottom panel of Figure 9, 908 positions were selected where both LRDS and LDS spectra were directly observed and where the deduced peak brightness temperatures agreed within 5%. The corresponding LRDS and LDS spectra were then compared (over the velocity range $-200 \leq V_{\rm LSR} \leq 100$ km s^{-1}) in order to ascertain the agreement in spectral shape, which should be related to the accuracy of the stray radiation corrections. The differences in T_b, in channels with $T_b > 10$ K, had an estimated standard deviation of 1.85 K or 6.5%, whichever is less, while the estimated σ in channels below this limit was 0.36 K. If one assumes that the uncertainties in *one* survey are 0.707 times these, the estimated uncertainty in one channel of the LRDS spectra increases to 0.25 K, and the distortion uncertainty increases to 4.6%.

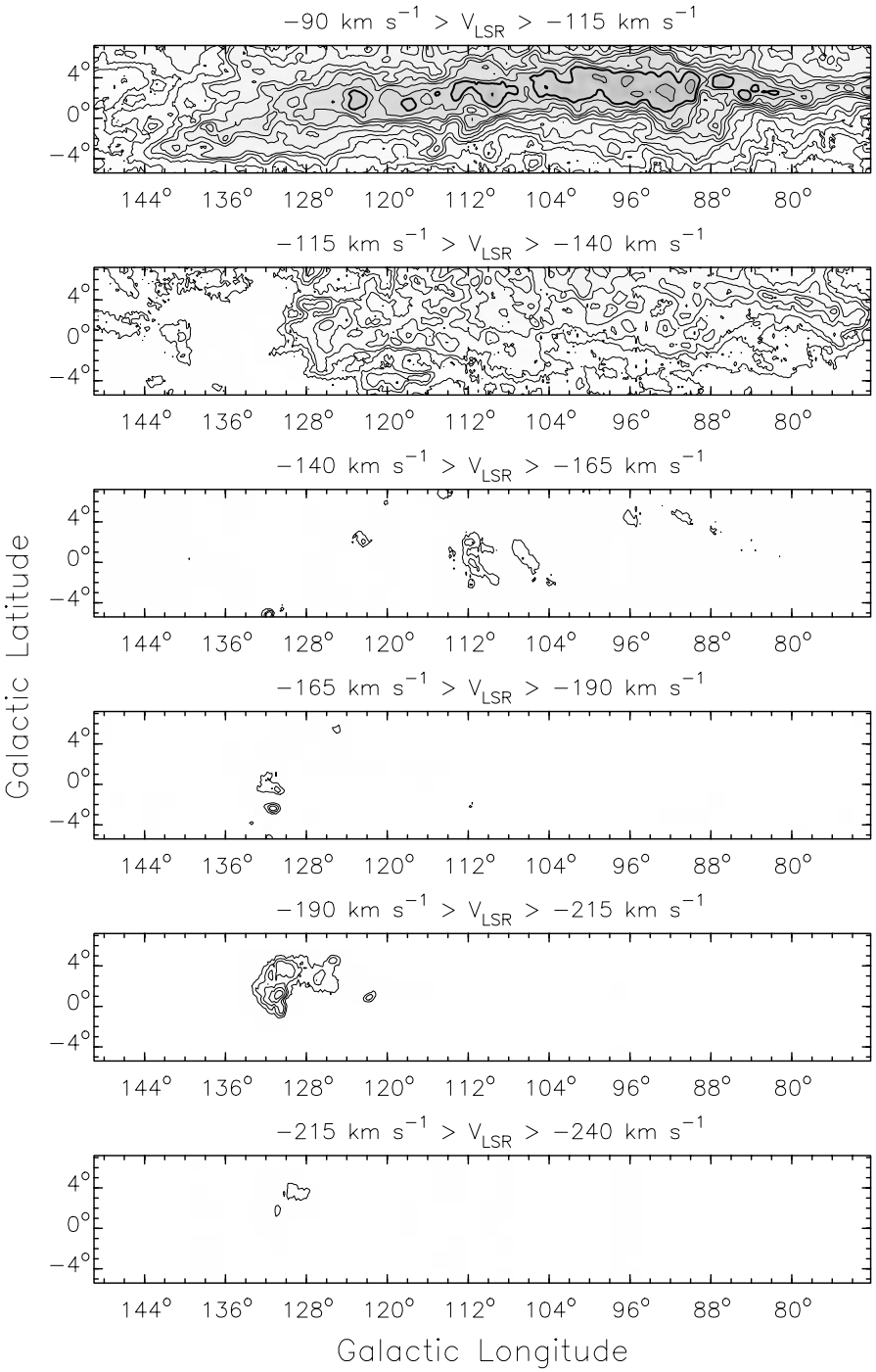

FIG. 17.—Integrated H I line intensity (K km s^{-1}) in six LSR velocity intervals, as a function of Galactic longitude and latitude. Contours are as in Fig. 16.

In some cases, spectra from the two surveys differ markedly, even though the peak line temperatures agree rather well. Two of the worst cases of this are shown in Figure 12. In each of these, the *ratios of spectral-line components* have changed. If these were "pointlike" components, pointing errors of about 8′ would be required to account for the discrepancies. Errors of this magnitude in either survey are unlikely. On the other hand, it is difficult to see how errors in the stray radiation corrections could produce such differences. There are rapid variations in line structure with position in both of these areas, so pointing problems may be indicated.

Obviously an independent, third survey would be useful in establishing better estimates of reliability of both the LRDS and the LDS.

6. A REGION OF STRONG H I SELF-ABSORPTION?

Although it is not the intent of this paper to extract new science from the survey data, one feature deserves comment. A statistic that has been found useful at DRAO in spectral

analysis is an estimate of rms noise on a spectrum deduced from simple first differences:

$$\sigma_{\rm est} = S\sqrt{\frac{\Sigma d_i^2 - (\Sigma d_i)^2/N}{N-1}}\,, \tag{3}$$

where

$$d_i = T_l(i) - 0.5 \times [T_l(i-1) + T_l(i+1)]\,, \tag{4}$$

and S is a constant depending upon the ratio of spectral resolution to channel separation.

This statistic will be increased in regions of greater spectral "complexity" and, in particular, in spectra which have very sharp features such as self-absorption dips. It was the use of this statistic that detected the two LDS spectra in Table 3 which have spurious features.

In both the LRDS and the LDS, the application of this statistic revealed a region of very notable "complexity," near $l = 92°$, $b = 3\overset{\circ}{.}5$. Spectra in this neighborhood all show a narrow absorption dip at $V_{\rm LSR} \sim -4$ km s^{-1}. This is illustrated in Figure 13 where a contour map of this statistic is shown along with one representative spectrum. This region, located to the Galactic northwest of the H II region CTB 102, appears to be one where widespread, strong H I self-absorption exists. It will be a prime area for CGPS studies of this phenomenon (Gibson et al. 2000).

7. DATA OVERVIEW AND AVAILABILITY

An overview of the survey results is given in Figures 14, 15, 16, and 17, in which the data have been averaged over longitude intervals and summed over velocity intervals.[1]

[1] The full survey data are available in FITS format from the DRAO public ftp site (ftp.drao.nrc.ca) or from the DRAO web site (http://www.drao.nrc.ca), following references to LRDS. Two FITS files are available, presenting the data in different fashions. Each, after compression by "gzip," is about 19 Mbytes in size. In the first (similar to Figs. 14 and 15), the data are presented as 512 channels of spectral data times 64 Galactic latitudes times 385 Galactic longitudes. In the second FITS file (similar to Figs. 16 and 17), the data are presented as 385 Galactic longitudes times 64 Galactic latitudes times 512 spectral channels.

8. CONCLUSIONS

A 975 deg^2 area of the northern Galactic plane has been observed in the H I line with good sensitivity. This is the first survey of this region with full spatial sampling (better than two samples per beamwidth). Considerable care has been taken in the calibration of the survey against the standard region S7. A complementary study of the antenna characteristics of the DRAO 26-m Telescope allowed corrections to be made for stray radiation. Although the survey was conceived as a means of providing "short-spacing" H I data for the CGPS, a valuable secondary application has been its comparison with the Leiden/Dwingeloo Survey, the "standard" H I survey of the Galaxy. This has shown that a very small fraction of the spectra in that survey suffer from previously undetected calibration errors, of up to 25% or more, and that caution should be taken in the use of individual spectra for quantitative research. Probably no more than 1% of the spectra in the LDS have calibration errors exceeding 10%.

We wish to thank Charles Kerton for major contributions in the determination of the antenna pattern and Diana Chaytor for making most of the survey observations. The Dominion Radio Astrophysical Observatory is operated as a national facility by the National Research Council of Canada. The Canadian Galactic Plane Survey is a Canadian project with international partners, and is supported by a grant from the Natural Sciences and Engineering Research Council of Canada.[2]

[2] Further details regarding the CGPS are available from the web site: http://www.ras.ucalgary.ca/CGPS.

APPENDIX A

SPECTRAL CALIBRATION PROCEDURE

The numerical spectrometer output (transformed correlator lag coefficients) in frequency channel i may be expressed as

$$V(i) = Kg(i)\Sigma[T(i)]\,, \tag{A1}$$

where $g(i)$ is the system gain in that channel, K is a constant depending upon bandwidth and the signal processing, and $\Sigma[T(i)]$ is the sum of all the antenna temperature components in that channel. The gain function $g(i)$ can be divided into two contributions: $W(i)$, the gain of the system common to the H I band and reference-band observations (for example, the gain of the receiver intermediate-frequency amplifiers), and $G(i)$, that part which is different for the two reception bands, such as the gain of the receiver front-end amplifiers. The antenna temperature consists of the system temperature T (due to receiver noise, ground and sky radiation, and any contribution from continuum radio sources), assumed constant over the observed frequency band, and an H I line component $T_l(i)$.

The outputs from the ith channel of the spectrometer, after averaging over eight 5.625 s intervals, for the H I band and reference-band observations can be expressed as

$$V_s(i) = KG_s(i)W(i)[T_l(i) + T_s]\,, \tag{A2}$$

and

$$V_r(i) = KG_r(i)W(i)T_r\,, \tag{A3}$$

where the subscripts s and r refer, respectively, to H I (signal-band) and reference-band observations.

When the calibration noise source (which adds noise with an effective antenna temperature T_c into the receiver input, assumed constant over both bands) is switched on, the two outputs become

$$V_{sn}(i) = KG_s(i)W(i)[T_l(i) + T_s + T_c] , \tag{A4}$$

and

$$V_{rn}(i) = KG_r(i)W(i)[T_r + T_c] , \tag{A5}$$

where the additional subscript n indicates that the noise source is switched on.

In the first stage of the calibration process, three calibration factors are derived from each noise observation. These are the relative-gain function $A(i)$ and the constants B and C:

$$A(i) = \frac{G_s(i)}{G_r(i)} = \frac{V_{sn}(i) - V_s(i)}{V_{rn}(i) - V_r(i)} , \tag{A6}$$

$$B = \frac{T_c}{T_r} = \left\langle \frac{V_{rn}(i) - V_r(i)}{V_r(i)} \right\rangle , \tag{A7}$$

and

$$C = \left\langle \frac{T_c}{T_s + T_l(i)} \right\rangle = \left\langle \frac{V_{sn}(i) - V_s(i)}{V_s(i)} \right\rangle \approx \frac{T_c}{T_s + \langle T_l(i) \rangle} , \tag{A8}$$

where angle brackets denote an average over the 512 spectrometer channels. A smoothed version of $A(i)$, together with constants B and C, were stored in the calibration database.

When a spectral observation is to be calibrated (into antenna temperatures expressed in units of T_c), the function $F(i)$ is computed:

$$F(i) = \frac{V_s(i)}{V_r(i)} . \tag{A9}$$

The relevant calibration factors are extracted from the calibration database and the calibrated spectrum is obtained from

$$\frac{T_l(i) - \langle T_l(i) \rangle}{T_c} = \frac{F(i)}{BA(i)} - \frac{1}{C} . \tag{A10}$$

The spectrum calibrated in this way would have a zero mean if the approximation in equation (A8) were an equality. Therefore, a small offset results.

From observations of the S7 spectrum, equation (A10) allows T_c to be converted to T_b^*. These values of brightness temperature of the noise signal were stored in a second database. Using these values, the observed LRDS spectra were converted to effective brightness temperature units.

APPENDIX B

REMOVAL OF INTERFERENCE

A simple "clipping" approach was used. First of all, an approximate value of the noise on the spectrum, $\sigma_{\rm est}$ (see eq. [3]), was determined from channel-to-channel variations. A 14 channel window was then stepped across the spectrum, and at each position of the window a two-stage algorithm was applied to find "discordant" intensities. In the first stage, a quadratic function, $Q(i)$, was fitted to the intensities in channels $i = 1$–6 and $i = 9$–14 within the window. Intensities in these 12 channels that deviated from $Q(i)$ by more than 3 $\sigma_{\rm est}$ were flagged to be "omitted" in the second stage. In the second stage, a new quadratic function, $Q'(i)$, was fitted to the remaining intensities. Using only those intensities which deviate from $Q'(i)$ by less than 3 $\sigma_{\rm est}$, a new noise estimate, $\sigma_{\rm quad}$, was derived.

If either of the intensities in channels 7 or 8 in the window deviated from $Q'(i)$ by more than $S \times \sigma_{\rm quad}$ (where S was normally 4), they were flagged as "discordant" and were replaced by the value given by $Q'(i)$, plus a noise component. The latter was randomly selected from a distribution with σ equal to the maximum of 0.5 $\sigma_{\rm est}$, $\sigma_{\rm quad}$, and 0.1 $\times$ ($Q'_{\rm max} - Q'_{\rm min}$). The latter term is 1/10 of the variation of Q' in the window.

To prevent the algorithm from flagging sharp spectral features as "interference," some modifications to the above parameters were made when the intensities in the windowed channels were above 4 K. The value of S increased with line intensity, doubling for channels at 50 K, and the removal of spikes greater than 2 K was inhibited.

APPENDIX C

ANTENNA TERMINOLOGY AND BASIC RELATIONS

The power pattern of the antenna is defined in terms of the angle θ_d and ϕ_d, where θ_d is the angle from the direction in which the antenna is pointing, and ϕ_d is an azimuthal angle measured counterclockwise, on the sky, from the direction to the north celestial pole. The antenna pattern is characterized by the function $f(\theta_d, \phi_d)$ which has a value of 1.0 at $\theta_d = 0.0$.

The integral of $f(\theta_d, \phi_d)$ over 4π sr is termed the antenna solid angle, Ω_A. The "main beam" of the antenna for the purpose of this paper is defined by $\theta_d < 1°$. Within this radius, a good approximation to the antenna pattern is a $\cos^6 \theta_d$ distribution, with half-power widths of $37'.0 \times 35'.3$, at a position angle of 156°. Similarly to the definition of antenna solid angle, the integral of the pattern over the main beam gives the main-beam solid angle, Ω_{MB}. The main beam of the DRAO 26-m Telescope, as defined above, has $\Omega_{MB} = 1.198 \times 10^{-4}$ sr.

Basic relations exist between the antenna aperture, A in square meters; the aperture efficiency, η_A; the directivity of the antenna, D_A; the radiative efficiency of the antenna, η_r, the gain of the antenna, G_A, and the antenna solid angle, Ω_A. The directivity is related to the antenna solid angle by

$$D_A = 4\pi/\Omega_A \, . \tag{C1}$$

The gain of the antenna is related to the directivity by

$$G_A = \eta_r \times D_A \, , \tag{C2}$$

where η_r reflects the effects of ohmic losses in the feed and antenna surface. Finally, the aperture efficiency, η_A, is defined by

$$\eta_A = G_A \lambda^2/(4\pi A) \, , \tag{C3}$$

where λ is the wavelength of observation, in meters; in this case, 0.211 m. If the DRAO 26-m Telescope ($A = 514.85$ m^2) were a "perfect" antenna, with $\eta_A = 1.0$, it would have a gain of 1.453×10^5 or 51.62 dB, at the wavelength of 21.1 cm.

The aperture efficiency can be considered to be the product of several other efficiency factors, including η_r, as follows

$$\eta_A = \eta_r \times \eta_{ill} \times \eta_{spo} \times \eta_{sw} \times \eta_l \times \eta_{ss} \times \eta_b \, , \tag{C4}$$

where the efficiencies are defined as follows:

The illumination efficiency, η_{ill}.—This would be 1.0 for a uniformly illuminated aperture, but in practice this value cannot be achieved because of the difficulty in obtaining uniform illumination. In addition, the need to minimize sidelobes entails deliberately tapering the illumination of the aperture.

The spillover efficiency, η_{spo}.—This is really the feed efficiency and would be 1.0 if the feed illuminated only the reflector surface.

The spherical-wave–scattering efficiency, η_{sw}.—This would be 1.0 if none of the radiation emitted from the feed (in a spherical wave), which is directed toward the reflector, were scattered by reflection from the feed-legs.

The leakage efficiency, η_l.—This would be 1.0 if no radiation falling upon the reflector leaked through the surface mesh but were all reflected.

The surface-scattering efficiency, η_{ss}.—This would be 1.0 if the reflector were a perfect paraboloidal mirror. Surface errors cause some of the radiation being reflected to be scattered out of the forward direction.

The blockage efficiency, η_b.—This would be 1.0 if the plane wave leaving the reflector surface in the forward direction met no obstacles such as feed-legs or focus box. These scatter radiation into other directions. In particular, the feed-legs scatter radiation into "scatter cones."

Two more relations define the "stray factor," β, of the pattern, and the beam efficiency, η_B. The former indicates the fraction of the response of the antenna that originates outside of the main beam and is defined by

$$\beta = (\Omega_A - \Omega_{MB})/\Omega_A \, . \tag{C5}$$

The beam efficiency is related to β by

$$\eta_B = \eta_r \times (1 - \beta) \, . \tag{C6}$$

REFERENCES

Gibson, S. J., Taylor, A. R., Higgs, L. A., & Dewdney, P. E. 2000, ApJ, 540, 851

Hanson, B. E. 1964, M.Sc. thesis, Dept. of Elec. Eng., Univ. of British Columbia

Hartmann, D., & Burton, W. B. 1997, Atlas of Galactic Neutral Hydrogen (Cambridge: Cambridge Univ. Press)

Hovey, G. J. 1998, M.A.Sc. thesis, Dept. of Elec. Eng., Univ. of British Columbia

Kalberla, P. M. W. 1978, Ph.D. thesis, Univ. of Bonn

Kalberla, P. M. W., Mebold, U., & Reich, W. 1980, A&A, 82, 275

———. 1982, A&A, 106, 190

Murphy, E. M. 1993, M.A. thesis, Dept. of Astronomy, Univ. Virginia

Numerical Electromagnetic Code: NEC–REF (Ver. 2), 1982. Tech. Rep. 712242-16 (713742), Ohio State Univ, US Dept. of Navy

Taylor, A. R., et al. 2000, in preparation

Wakker, B. P., & van Woerden, H. 1991, A&A, 250, 509

Weaver, H., & Williams, D. R. 1973, A&AS, 8, 1

Williams, D. R. 1973, A&AS, 8, 505